Analyst

ROYAL SOCIETY
OF CHEMISTRY

PAPER
Tim Thomay *et al.*
Utilizing quantum fingerprints in plant cells to evaluate plant
productivity

150 YEARS
ANNIVERSARY

Check for updates

Utilizing quantum fingerprints in plant cells to evaluate plant productivity

Umadini Ranasinghe, [ID] †[a] Abigail L. Stressinger, [ID] †[b,d] Guangpeng Xu, [ID][a] Yasmin Sarhan, [ID][a] Fred Harrington,[c] James O. Berry [ID][b] and Tim Thomay [ID] *[a]

Overcoming the strong chlorophyll background poses a significant challenge for measuring and optimizing plant growth. This research investigates the novel application of specialized quantum light emitters introduced into intact leaves of tobacco (*Nicotiana tabacum*), a well-characterized model plant system for studies of plant health and productivity. Leaves were harvested from plants cultivated under two distinct conditions: low light (LL), representing unhealthy leaves with reduced photosynthesis and high light (HL), representing healthy leaves with highly active photosynthesis. Higher-order correlation data were collected and analyzed using machine learning (ML) techniques, specifically a Convolutional Neural Network (CNN), to classify the photon emitter states. This CNN efficiently identified unique patterns and created distinct fingerprints for *Nicotiana* leaves grown under LL and HL, demonstrating significantly different quantum profiles between the two conditions. These quantum fingerprints serve as a foundation for a novel unified analysis of plant growth parameters associated with different photosynthetic states. By employing CNN, the emitter profiles were able to reproducibly classify the leaves as healthy or unhealthy. This model achieved high probability values for each classification, confirming its accuracy and reliability. The findings of this study pave the way for broader applications, including the application of advanced quantum and machine learning technologies in plant health monitoring systems.

1 Introduction

Autofluorescence, the natural light emission from plant tissues, poses a significant obstacle in accurately studying their fluorescent properties, sometimes leading to inaccurate determinations of photosynthetic activity.[1–3] This phenomenon, primarily driven by chlorophyll emissions and other light gathering proteins,[4] can be affected by multiple variable factors, including quenching and overlapping signals, making it difficult to quantify and standardize the multiple parameters associated with overall photosynthetic health and productivity. Quantum dots (QDs), with their unique property of emitting only one photon at a time, help to overcome this strong chlorophyll fluorescence commonly found in plants.

Due to their distinctiveness of light, QDs as quantum light emitters are highly specific and reflective of their surrounding conditions. Therefore, quantum light from QD-transformed species is reflective of the environmental and intracellular conditions of the organism. This property has led to the use of quantum dots in plant systems,[5] primarily as enhancers of productivity and biosensors for pathogen and pollutant detection.[6] Furthermore, QDs have been utilized to monitor nutrient levels in plants, providing critical insights into their nutritional status and enabling nutrient management strategies.[7–9] Most recent applications have focused on utilizing QDs to mitigate abiotic stressors and enhance plant growth.[6,10–14] As quantum light emitters, QDs have the ability to monitor plant health and distinguish sub-optimal growth conditions. Yet, minimal research has been conducted on the role of QDs as evaluators of plant productivity.

Understanding how QDs are used as quantum light emitters requires first recognizing how the concept of light as discrete energy quanta has led to advancements in studying photon number properties. These developments have established a foundational concept central to our current quantum optics experiments. In an early 1956 study, Hanbury Brown and Twiss[15] conducted a groundbreaking experiment that distinguished between thermal and Poissonian light, marking a pivotal moment in the study of optical coherence. This foundation was further established in a 1963 study by Glauber and Sudarshan[16,17] introduced the quantum theory of photon correlations. Their work focused on higher-order factorial

[a]Department of Physics, State University of New York at Buffalo, New York, USA. E-mail: thomay@buffalo.edu
[b]Department of Biology, State University of New York at Buffalo, New York, USA
[c]Helios-NRG, LLC, East Amherst, New York, USA
[d]Department of Environment and Sustainability, State University of New York at Buffalo, New York, USA
† These authors contributed equally to this work.

moments of photon-number distributions, providing a framework to analyze and understand the behavior of light at the quantum level.[5,16–18] Their findings set the stage for advancements in understanding the properties of light sources, bridging classical and quantum optics.

The exploration of higher-order photon correlations has since led to numerous applications, particularly in quantum light emitters.[19,20] Furthermore, this technology can be used in a range of biological applications.[21,22] Most notably, photon correlation techniques have been applied in cancer diagnostics. Detecting and treating cancer remains a major challenge in medicine. Optics and photonics technologies have applied principles of physics to enhance diagnostic methods.[23] Furthermore, photon correlation spectroscopy (PCS), a specialized technique within photon correlation that analyzes fluctuations in scattered light to determine the size and motion of particles in a sample, has been used to study proteins and other biomacromolecules in aqueous solutions. PCS has been widely applied to investigate conformational changes in proteins, their aggregation, and interactions with other molecules. These studies help to reveal important native functions of proteins, DNA, RNA, and even microorganisms like *Escherichia coli*, *Pseudomonas putida*, and *Dunaliella viridis*.[24,25] Furthermore, time correlated single photon counting (TCSPC) is a technique that detects single photons from a periodic light signal, records their detection times, and creates a distribution of photons over the signal's time period. This technique has numerous biomedical applications, such as time-domain optical tomography, studying transient phenomena in biological systems, spectrally resolved fluorescence lifetime imaging, fluorescence resonance energy transfer (FRET) experiments in live cells, and analyzing dye-protein complexes using fluorescence correlation spectroscopy.[26–28] However, there has been limited research exploring photon correlation in plants.

In the past decade, data-driven approaches like Machine Learning (ML) have opened up new opportunities for quantum photonics experiments.[29–32] ML models, known for handling large and sparse datasets, have achieved significant speedups in certain quantum measurements[29,33–35] and offer a way to overcome the limitations of traditional fitting methods, especially in the low-photon flux regime.[36–39] One notable advancement is the development of a Convolutional Neural Network (CNN)-based algorithm tailored for the rapid classification of single-photon emitters within the nitrogen-vacancy (NV) center of nanodiamonds.[40–43] The CNN model improves accuracy by identifying subtle features extracted from sparse correlation data.

Logistic regression is a machine learning classifier used when the outcome is categorical, most commonly binary (for example, "success" *vs.* "failure"). It fits a sigmoid function to a linear combination of input features to estimate class probabilities, with parameters chosen to maximize the likelihood of the data. In contrast, *t*-tests are a family of statistical hypothesis tests used to compare the means of continuous data. A one sample *t*-test determines whether a sample mean differs from a known value. An independent (two-sample) *t*-test compares the means of two separate groups, while a paired *t*-test looks at the means from the same group under two different conditions. Logistic regression and *t*-tests are limited to simple, linear, or single variable comparisons, while CNN can automatically learn complex, multi-level feature patterns.[44,45]

In this study, we aim to develop an innovative technique to optimize plant productivity using a novel quantum-based fingerprinting concept. The approach involves introducing biocompatible quantum dots (QDs) as quantum light emitters into the leaf cells of tobacco plants. Plants were grown under two distinct environmental conditions, low light (LL) and high light (HL), to assess the technique's applicability across different growth scenarios. We hypothesize that QDs as quantum light emitters provide a significant advantage over methods using classical chlorophyll fluorescence detection, which are often masked by plant pigments and light-absorbing/quenching components in photosynthetically-active plant tissues.[2–4,46] Quantum light sources emit single photons with unique quantum properties, allowing them to be optically distinguished from classical multiphoton light sources. This optical quantum differentiation is achieved by leveraging higher-order correlation functions to analyze and confirm the quantum nature of the emitted light. To interpret the data, we classify the quantum signals based on time resolved correlation patterns using a Convolutional Neural Network (CNN) model. The CNN is trained to extract subtle and complex features from the data, enabling it to accurately differentiate between the quantum properties of light that are emitted from healthy and unhealthy leaves. This is done without interference from any other non-quantum light emissions within the experimental leaf samples. This approach results in the creation of distinct quantum fingerprints for each leaf, representing their unique quantum fluorescence characteristics. Furthermore, we show that our pre-trained machine learning model can classify the probabilities of emissions from experimental categories, thereby predicting the derived quantum fingerprints as being from healthy or unhealthy leaves. The results show that quantum-based fingerprinting provides a novel and effective way to characterize optimal plant growth and monitor plant health under different conditions.

2 Method

2.1 Preparation of leaves and analysis of photosynthesis

Tobacco (*Nicotiana tabacum* var. SR1) leaves were prepared under low-light (LL) conditions and high-light (HL) conditions. All growing conditions were standardized in growth chambers (24 °C, 12 h light/dark cycle, daily watering) except for light intensity, which differed by 30 Å between groups. The high-light group was exposed to 430 μmol photons per m^2 per s (430×10^{-6} Einstein per m^2 per s), and the low-light group received only 15 μmol photons per m^2 per s (15×10^{-6} Einstein per m^2 per s) of light. Normal growth light conditions for tobacco plants are between 400–450 μmol m^{-2} s^{-1} ($400–450 \times 10^{-6}$ Einstein per m^2 per s).[47] LL conditions significantly

decrease rates of photosynthesis, leading to reductions in growth, stomatal conductance, intercellular carbon dioxide levels, and transpiration rates.[48,49] As a result, the LL group is considered unhealthy compared to the HL group, which is expected to affect quantum measurements.

To determine the photosynthetic efficiency of each experimental group, we used the PhotosynQ MultispeQ V 2.0 fluorimeter device (Photosynq Inc. East Lansing, MI 48823 USA). The following parameters were analyzed for each tobacco leaf: photosynthetically active radiation (PAR), non-photochemical quenching, relative chlorophyll, and photosystem I active centers. PAR was calculated by measuring the fraction of incoming light that is active in promoting photosynthesis.[50] Non-photochemical quenching infers plant health by measuring the plant's ability to dissipate excess light energy harmlessly as heat and is calculated by providing pulse-amplitude modulation fluorescence. The chlorophyll content of each leaf was calculated by measuring the ratio between the absorbance of red (650 nm) and infrared (940 nm) light. Finally, the number of active Photosystem I centers was determined by absorbance-based measurements (810–940 nm).

These parameters provide a quantitative measurement of the overall photosynthetic efficiency of each experimental group of tobacco leaves. A total of sixteen leaves, eight from each experimental group, were measured for this study. For each of the 16 leaves, four separate photosynthesis parameters (PAR, chlorophyll content, quenching, and Ps1 activity) were measured, with all parameters indicating a reduction in photosynthetic activity under reduced lighting. For each of the two growing conditions, there are 32 total photosynthesis measurements, which clearly confirm a reduction in photosynthesis in the LL experimental group. All measurements were collected using the PhotosynQ 2.0 MultispeQ device, a handheld pulse amplitude modulated chlorophyll fluorometer and multispectral sensor. Each photosynthetic parameter was measured twice, providing two technical replicates for each leaf (biological replicate). This provided an optimal framework for assessing photosynthetic function under the two growth conditions.[51]

2.2 Biolistic transformation of leaves

Tobacco leaves were transformed using the Biolistic PDS-1000/He Particle Delivery System, commonly known as the "Gene Gun" (Bio-Rad PDS-1000/He). This system was used to deliver custom gold microprojectiles coated with DNA and quantum dots onto the abaxial surface of each tobacco leaf. We modified previously published protocols for transformation of tobacco plants.[52,53] To prepare the microprojectiles, we added 0.1 M Biotin-PEG-SH-Thiol (Nanocs MW 5000) to 20 μl of 66 nm gold particles (Bio-Rad), creating a conjugated gold-biotin particle. Green fluorescent protein (GFP) report gene was delivered via the pBI121-GFP vector of a constitutive CaMV35S promoter.[54] The GFP plasmid was added in a ratio of 10 μg DNA to 1.2 mg of gold-biotin particles. The particles were combined with 25 μl of 2.5 M CaCl$_2$, 10 μl of 0.1 M spermidine free base, then vortexed for 15 seconds. The DNA-coated microprojectiles were centrifuged at maximum speed for 5 seconds, washed with

100% EtOH, and resuspended in 24 μl 100% EtOH. Finally, 5 μl of Streptavidin Conjugate CdSe/ZnS core/shell Quantum Dots (585 nm, Invitrogen Thermo Fisher Scientific) were added to the particle solution. This linked the quantum dots to the gold microprojectile via the Biotin-PEG-SH-Thiol linker as shown Fig. 1.

After being detached from their host plant, each tobacco leaf was bombarded twice at 900 psi by 8 μl of microprojectiles. Stopping screens were placed 6 cm away from the Petri dish containing the leaf. After bombardment, leaves recovered in the dark for 24 hours, then were moved back to their initial growth chambers prior to examining for GFP expression and quantum fluorescence.

2.3 Development of quantum fingerprint

The photoluminescence (PL) of leaves was measured to confirm the emission of QDs. A Hanbury-Brown and Twiss (HBT) setup with four detectors is shown in Fig. 2. It was used to measure second-order correlation that describes the probability of detecting two photons at different times, providing information about the photon emission statistics. This work expands upon previous findings,[55] where an HBT setup is employed to study photon correlation properties. Each path leads to an Avalanche Photodiode (APD). Every photon that arrives at the APD triggers a click recording the detection time.

Higher-order correlation data were collected and analyzed using a machine learning model to classify the photon states. Further details on the computational method can be found in.[56] The correlation data was compiled into a 3D matrix with dimensions $(4,4,2x + 1)$, where x is the bin number. Starting with $x = 6$, the resulting matrix has dimensions $(4,4,13)$, representing the $g^{(2)}$ correlation matrix. Each pairwise $g^{(2)}$ curve was segmented into fixed length blocks of 13 delay bins, producing input tensors of size $4 \times 4 \times 13$ per sample. Before being processed by CNN, each tensor was min-max normalized to the interval [0, 1]. The 13 bin segmentation adheres to established
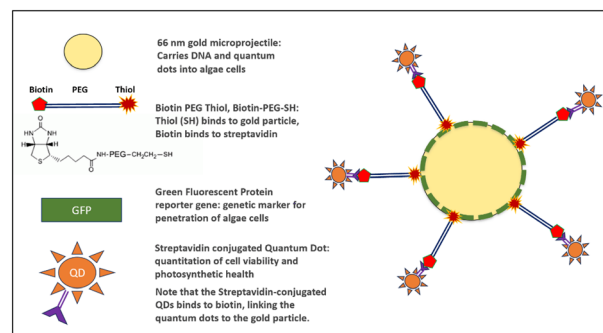
Fig. 1 Design of a multi-component gold projectile designed to carry DNA and QDs into plant cells. Biotin PEG Thiol serves as a linker between the gold microparticle and QDs. Green Fluorescent Protein (GFP) serves as a visible genetic marker for successful cellular uptake, which, when expressed, fluoresces green under ultraviolet light. Streptavidin-conjugated QDs (emission spectrum of 585 nm) fluoresce orange under ultraviolet light.
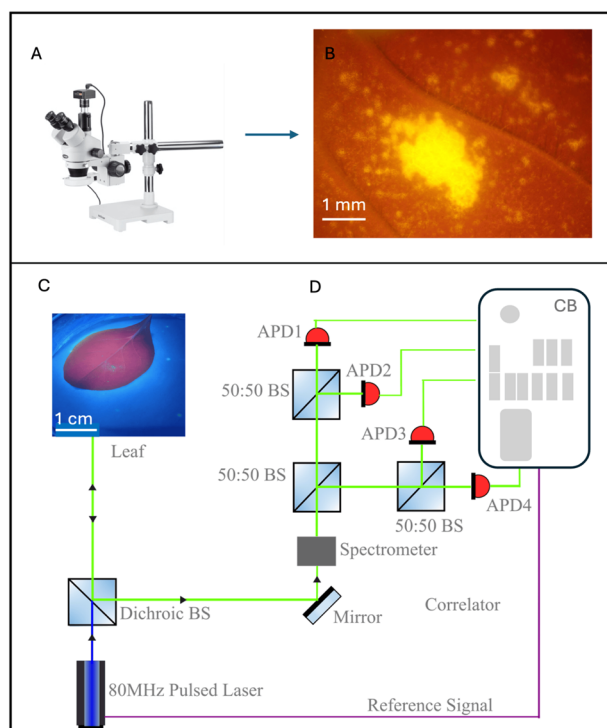
Fig. 2 Experimental layout for measuring higher-order correlation. (A) The leaf under 365 nm UV light (B) the stereo microscope (C) the leaf under stereo microscope (D) the Hanbury Brown and Twiss (HBT) set up with 50:50 Beam Splitters: BS, and detected by Avalanche Photodiodes: APDs connected to a Correlation Board: CB.

quantum correlation measurement protocols, striking a balance between finite duration normalization artifacts at large bin widths which can produce unphysically low $g^{(2)}$ values and overestimation due to photon bunching at very short bin widths.[57] Other segment lengths (n = 4, 5, 6, 7, 8) were also evaluated, refer to Fig. S1 in the SI for more details.

Each sample in our experiment yields a $4 \times 4 \times 2001$ correlation tensor, based on second-order photon correlation functions $g^{(2)}(\tau)$ for all $\binom{4}{2} = 6$ unique detector pairs (from four APDs) over 2001 time bins. This produces $4 \times 4 \times 2001 = 12\,006$ correlation values per leaf, which encode rich temporal and spatial information sensitive to plant health.

We then partition each full correlation tensor into multiple segments of shape $4 \times 4 \times 13$, resulting in hundreds of informative correlation blocks per leaf. These blocks serve as independent inputs to our CNN. The sample size was determined in accordance with established biological standards, yielding a dataset of correlation fingerprints that is both significantly larger and structurally rich.[51]

This matrix forms the foundation for creating a 2D quantum fingerprint in tobacco leaf cells by normalizing the matrix.

2.4 Classification of probabilities

The convolutional neural network (CNN) utilized in this study was designed for binary classification based on quantum fin-

gerprint data. The model starts with a Conv2D layer that includes 16 filters with a 3 Å3 kernel size and uses ReLU activation to help extract local spatial features from the input data. Following this, a Flatten layer reshapes the 2D feature maps into a 1D vector, making it suitable for the dense layers.

In the dense section of the network, there is a hidden layer containing 32 neurons with ReLU activation, followed by a final output layer with a single neuron using sigmoid activation to predict the binary class (*e.g.* HL *vs.* LL leaf). The model was trained using the Adam optimizer and binary cross-entropy as the loss function. Training was conducted for up to 20 epochs, with early stopping enabled to prevent overfitting. A batch size of 1, appropriate for the dataset size was used, and 20% of the data was reserved for validation during training.

We validated CNN's generalization using a strict leaf-level hold-out instead of *k*-fold cross-validation or repeated runs. This approach ensured that we did not mix data from the same physical leaf between the training and testing sets.

After training, the model was used to classify leaves by predicting probabilities for each sample as either healthy or unhealthy, providing a clear indication of its confidence in each classification. To further validate its performance, the trained model was tested on new, unseen data, where it successfully assigned probabilities to each sample in the validation set, determining whether a leaf is healthy or unhealthy. The model architecture and layer operations are illustrated in Fig. 3.

3 Results

This study combines quantum technology and machine learning to analyze plant health productivity. Quantum dots (QDs) were introduced into tobacco leaves to study their quantum properties under different lighting conditions. The data revealed clear differences between healthy and unhealthy leaves, visualized as unique quantum fingerprints. The CNN model accurately classified the leaves, achieving high probabil-
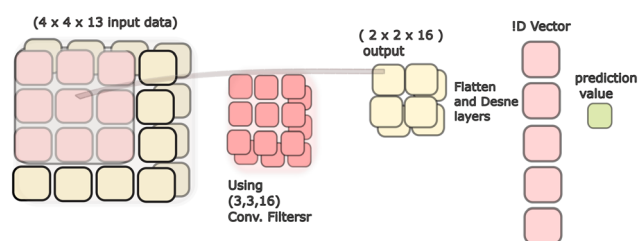
Fig. 3 Schematic of the CNN model for probability classification. The architecture consists of a convolutional layer, followed by a Conv2D layer with 16 filters and a (3 Å3) kernel, activated using ReLU. A flattening layer converts the convolutional output into a 1D feature vector. The model includes dense layers for binary classification: one with 32 neurons and ReLU activation to learn complex feature representations, and a final dense layer with a single neuron and sigmoid activation for classification.

ities for both HL and LL categories, demonstrating the effectiveness of this approach in plant health productivity.

To determine the productivity of tobacco leaves on a cellular level, we measured photosynthetic parameters based on light-driven fluorescence and absorbance changes *via* LED light. As expected, the tobacco plants used in this experiment, which were grown under reduced light intensity, exhibited lower rates of photosynthesis. Thus, the parameters for tobacco grown under HL will have high photosynthetic activity than plants grown under LL. Overall, we observed statistically significant differences in all parameters between HL and LL tobacco leaves (Fig. 4). Therefore, tobacco leaves from both experimental groups have contrasting rates of photosynthesis, which will be reflected in their quantum fingerprint.

The gold microprojectiles were specifically engineered to serve as carriers for both DNA and QDs into the tobacco plant cells. This design successfully allowed for the microcarrier and its components to gain cellular entry through biolistic transformation. Our constructed microprojectile links biocompatible quantum dots and Green Fluorescent Protein (GFP) reporter gene to gold nanoparticles as shown in Fig. 1. Therefore, the GFP marker serves as a confirmation of delivery of the microprojectile into tobacco leaf cells. When the GFP reporter gene entered the cell nucleus, green fluorescence was observed under ultraviolet light, indicating the entry of all components, including streptavidin-conjugated quantum dots (Fig. 5). Additionally, orange fluorescence was observed on both HL and LL leaves, confirming the presence of quantum dots. Both green and orange fluorescence was observed in HL and LL leaves.

The successful emission of QDs was confirmed through a photoluminescence spectrum, as illustrated in Fig. 6. The plot highlights distinct emission peaks corresponding to the key components introduced into the tobacco leaf cells.
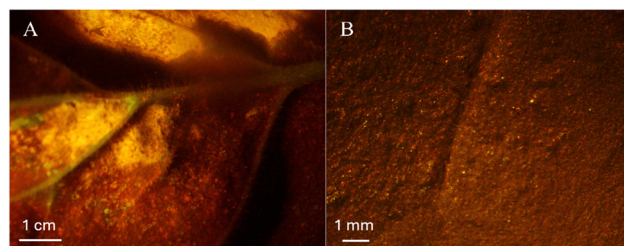
Fig. 5 Successful delivery of a multi-component microprojectile into tobacco leaf cells facilitated introduction of quantum dots. (A) Stereoscope image of a HL tobacco leaf under ultraviolet light (365 nm) shows strong GFP and quantum dot fluorescence. (B) Stereoscope image of a LL tobacco leaf under ultraviolet light (365 nm) also shows GFP and quantum dot fluorescence, confirming successful microprojectile penetration.
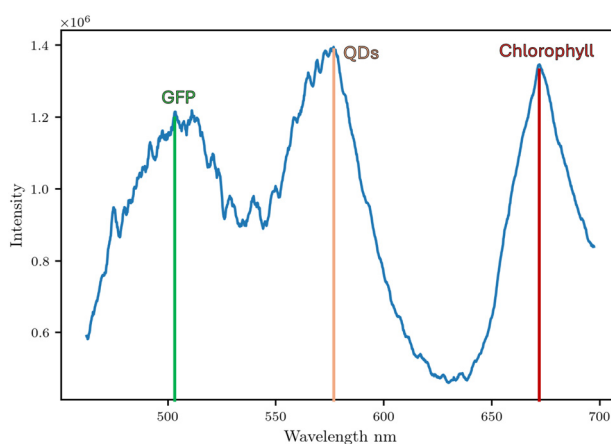
Fig. 6 Photoluminescence (PL) spectrum of the tobacco leaf showing distinct emission peaks for Green Fluorescent Protein (GFP) at 500 nm, quantum dots (QDs) at 585 nm, and chlorophyll at 680 nm.
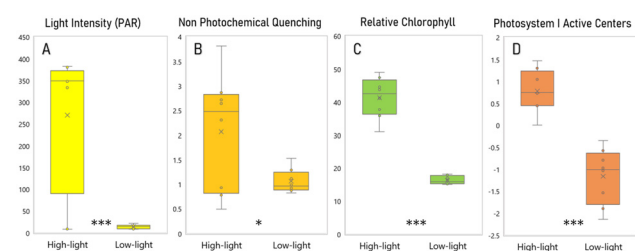
Fig. 4 Fluorescence and absorbance-based photosynthetic parameters indicate higher photosynthetic activity in HL *vs.* LL tobacco leaves. (A) Light intensity *via* photosynthetically active radiation (μmol photons per m^2 per s). (B) Non-photochemical Quenching measures each leaf's ability to dissipate excess absorbed light energy as heat. (C) Relative chlorophyll content (μmol of chlorophyll per m^2 of leaf), calculated by measuring the absorbance at 650 and 940 nm. (D) The fraction of Photosystem I centers that are active is calculated *via* a ratio of F_o (fluorescence level of a dark-adapted leaf with all Photosystem acceptors fully oxidized) to F_m (the maximum fluorescence achieved when all acceptors are fully reduced). This ratio is typically between 0.75 and 0.85 for healthy/light-sufficient leaves. Statistical significance is determined by a two-sample equal variance *t*-test: (*$p < 0.05$), (**$p < 0.01$), (***$p < 0.001$).

Specifically, the GFP exhibited a strong peak around 500 nm, indicating successful expression within the plant cells. The QDs displayed a prominent emission peak at 585 nm, verifying their presence and functionality as quantum light emitters. Additionally, a characteristic chlorophyll fluorescence peak was observed at approximately 680 nm, reflecting the natural autofluorescence of the plant. These well-defined peaks confirm the successful integration and activity of both GFP and QDs within the leaf cells, alongside the expected chlorophyll fluorescence background.

We generated four quantum fingerprints for leaves under LL and HL, as illustrated in Fig. 7. The data showed noticeable differences between tobacco plants with low and high-light conditions demonstrating the impact of photosynthetic activity on the quantum properties of the emitted light. The fingerprint is visualized as a 4 × 4 2D plot, where each detector pair correlation contributes 13 data points. These points appear as small rectangles on the plot, resulting in 208 segments across the entire plot. The diagonal elements always show zero as they represent correlations between the same detectors, and
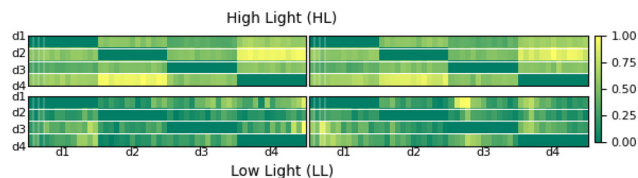
Fig. 7 Quantum fingerprints for healthy leaf grown in HL conditions (top), and an unhealthy leaf grown in LL conditions (bottom).

Table 1 Validation results for healthy and unhealthy leaves

Validation type	Time/step	Healthy probability	Unhealthy probability
Healthy validation leaf	0 s 54 ms per step	0.91	0.09
Unhealthy validation leaf	0 s 46 ms per step	0.16	0.84

the off-diagonal elements represent the time correlation values between different detector pairs.

These results suggest that quantum readings are affected by differences in photosynthetic productivity and health status. Using a novel quantum-based fingerprinting concept, we developed a higher-order photon correlation to optimize plant productivity.

The probabilities of the healthy and unhealthy validation leaves are summarized in Table 1. The model predicted a 91% probability of being HL and a 9% probability of being LL for the healthy validation leaf. Similarly, it predicted an 84% probability of being unhealthy and a 16% probability of being healthy for the unhealthy validation leaf.

Our results are based on the classification of correlation blocks, with the final accuracy reflecting the model's ability to distinguish between different health states at the block level rather than on a per-leaf basis. To prevent overfitting and enhance generalization, we employed several regularization strategies. First, we implemented early stopping to halt training once the validation loss stopped improving, ensuring that the model did not learn from noise. We also used a batch size of 1, which maximizes data diversity in each gradient update, an approach that is particularly important given the limited dataset. Additionally, we applied data normalization to ensure that all input features are on a consistent scale, which supports stable and efficient model training.

This confirms the accurate identification of leaves as healthy or unhealthy using the CNN model.

Ongoing experiments aim to explore further the link between quantum profiles and the optimization of productivity of tobacco plants.

4 Conclusions

Our study demonstrates the potential to link quantum data to plant photosynthetic health under varying growth conditions,

revealing significant differences between high-light (HL) and low-light (LL) environments. Light intensity, the critical growth condition we altered, significantly affected several photosynthetic parameters. The intensity of incoming light was directly related to the amount of light used for photosynthesis, and the ability to dissipate excess light energy as heat. As expected, chlorophyll content was also directly related to light intensity, since chlorophyll is the primary light-capturing molecule in plants and the activity of Photosystem I was more efficient in HL leaves. Photosystem I activity infers that HL leaves are healthier since they have a higher fraction of molecules converting light into chemical energy. Though the photosynthetic parameters we analyzed do not provide an overall measurement of photosynthetic activity for a plant, they establish a baseline indication of plant photosynthetic state. Incorporation of photosynthetic parameters such as stomatal conductance, electron transport rate, and protein and enzyme activity would create a more comprehensive measurement of plant health.[58,59] Correlating the combined, synergistic effects of these parameters with quantum profiles will further train our machine learning algorithm, and correlate plant responses to environmental stressors.

QDs introduced into the tobacco showed different quantum emissions under the two growth conditions, HL (more photosynthetically active) *versus* LL (less photosynthetically active), reproducibly responding quantitively to overall levels of photosynthesis in leaves of plants grown under the two light conditions. At this stage, we have not identified specific photosynthetic pathways, components or cell compartments that are affecting the overall quantum emissions. Photosynthesis is a complex process, involving a number of biochemical reactions, including the initial energy/redox-generating photosynthetic electron transport (PET) and photosynthetic carbon reduction (PCR, Calven-Benson), as well as downstream metabolic pathways.[46] Together these involve multiple cell compartments and structures (cytoplasmic, chloroplast, and mitochondria). Many of these processes are membrane-bound, others are soluble.[46] In cellular systems Quantum dot emissions are very dependent on their physical location surrounding environment.[60–64] Due to the non-specific Biolistic delivery system into intact leaves, it is likely that the overall QD emissions detected were a combined effect generated from different cell compartments, biochemical structures, and biochemical pathways associated with reduced photosynthetic function under the two plants growth conditions. Continuing experiments will involve specific targeting of QDs to specific structures, such as membranes, as well as linking the QDs to specific photosynthetic proteins, such as ATPase, electron transport components, redox-associated and carbon metabolism enzymes, using methods incorporated into many other studies and organisms.[60,61] In this way, this first general assay can be refined for analysis of specific photosynthetic processes affected by biotic or abiotic effectors.

An important feature of our approach is that quantum dot photon emissions are inherently stochastic and memoryless: each emission event is independent of the previous one. This

property has been widely exploited in the field of quantum random number generation, where the independence of successive photon detection events provides true physical randomness. Herrero-Collantes and Garcia-Escartin[65] provided an expansive review article covering the field. When constructing second-order correlation functions $g^{(2)}(\tau)$, we bin these independent photon events into time delays. Segmenting the correlation functions into shorter blocks therefore yields statistically independent realizations of the emission process, rather than correlated subdivisions of a continuous curve at very short times, photon bunching can occur, a well-known feature in quantum optics. This is one reason we chose to segment the correlation curves, since short-time structure provides additional quantum information, particularly for solid-state emitters where environmental coupling and blinking can play a role.[66] In support of this perspective, we have also recently demonstrated that machine learning models can analyze higher-order Fock state statistics to categorize different types of light including random, coherent, and quantum light providing a robust framework for extracting meaningful features from quantum emission data.[67] While the total number of biological replicates constrains the broader generalization of our study, segmentation provides multiple statistically independent realizations of the emission process, which serve as valuable inputs for CNN training without overstating the effective biological sample size.

Our findings provide a new method for correlating quantum light from quantum dots to photosynthesis in tobacco plants, which offers a novel way for monitoring plant health. Our results encourage further research on species with significant applications in agriculture, due to the heightened frequency and intensity of environmental conditions. As part of our future plan, we aim to refine and expand the approach to analyze a wider variety of plants and algae, including those from different species and under diverse environments as well as a range of abiotic and biotic stress conditions. These include, but are not limited to, water-depletion, extreme heat, chemical-contaminated soils, and pathogen-infection, all of which can affect photosynthetic function.[46] By advancing the integration of quantum technology and machine learning, this research lays the groundwork for innovative approaches to monitoring and improving plant productivity. Furthermore, we expect the Biolistic/QD analytical system described here will be expandable from laboratory conditions to field work, using the portable HeliosTM gene gun system.[68,69] This portable biolistic system does not require a vacuum and uses a hand-held delivery gun that can target coated microprojectiles into leaves and other specific tissues on intact plants.[70–72]

Author contributions

Umadini Ranasinghe: data curation, formal analysis, writing – original draft, writing – review & editing. Abigail L. Stressinger: sample preparation, data curation, writing – original draft, writing – review & editing. Guangpeng Xu: data curation, machine learning. Yasmin Sarhan: machine learning. Fred Harrington: data curation. James Berry: conceptualization, methodology, funding acquisition, supervision, project administration, visualization, writing – original draft, writing – review & editing. Tim Thomay: conceptualization, funding acquisition, supervision, project administration, visualization, writing – original draft, writing – review & editing.

Conflicts of interest

There are no conflicts to declare.

Data availability

Data for this article, including time tangled photon data, are available at Dryad Digital Repository at https://doi.org/10.5061/dryad.1rn8pk15f.

Supplementary information is available. See DOI: https://doi.org/10.1039/d5an00326a.

Acknowledgements

References

1 E. Murchie and T. Lawson, *J. Exp. Bot.*, 2013, **64**, 3983–3998.
2 K. Maxwell and G. N. Johnson, *J. Exp. Bot.*, 2000, **51**, 659–668.
3 T. Lawson and S. Vialet-Chabrand, *Methods in Molecular Biology*, Springer US, 2024, pp. 293–316.
4 N. C. M. Magdaong and R. E. Blankenship, *J. Biol. Chem.*, 2018, **293**, 5018–5025.
5 R. J. Glauber, *Phys. Rev.*, 1963, **130**, 2529–2539.
6 Y. Liu, L. He, A. Mustapha, H. Li, Z. Hu and M. Lin, *J. Appl. Microbiol.*, 2009, **107**, 1193–1201.
7 V. Ghormade, M. V. Deshpande and K. M. Paknikar, *Biotechnol. Adv.*, 2011, **29**, 792–803.
8 L. R. Khot, S. Sankaran, J. M. Maja, R. Ehsani and E. W. Schuster, *Crop Prot.*, 2012, **35**, 64–70.
9 R. Liu and R. Lal, *Sci. Total Environ.*, 2015, **514**, 131–139.
10 L. Chen, L. Zhu, X. Liu, L. Chen, H. Zhou, H. Ma, G. Sun, A. Nyande, Z. Li and H. Wu, *Crop J.*, 2024, **12**, 1274–1279.
11 A. R. Khan, A. Salam, G. Li, B. Iqbal, Z. Ulhassan, Q. Liu, W. Azhar, F. Liaquat, I. H. Shah, S. S. ul Hassan and D. Du, *Crop J.*, 2024, **12**, 1280–1298.
12 Y. O. Oyebamiji, B. A. Adigun, N. A. A. Shamsudin, A. M. Ikmal, M. A. Salisu, F. A. Malike and A. A. Lateef, *Horticulturae*, 2024, **10**, 156.

13 D. Tripathi, M. Singh and S. Pandey-Rai, *Plant Stress*, 2022, **6**, 100107.

14 R. Yan, Y. Zhang, H. Tian, Y. Hao and H. Sun, *Land Degrad. Dev.*, 2024, **35**, 3745–3755.

15 R. H. Brown and R. Q. Twiss, *Nature*, 1956, **177**, 27–29.

16 R. J. Glauber, *Phys. Rev. Lett.*, 1963, **10**, 84–86.

17 E. C. G. Sudarshan, *Phys. Rev. Lett.*, 1963, **10**, 277–279.

18 K. Laiho, T. Dirmeier, M. Schmidt, S. Reitzenstein and C. Marquardt, *Phys. Lett. A*, 2022, **435**, 128059.

19 S. Powers, G. Xu, H. F. Fotso, T. Thomay and D. Stojkovic, *arXiv* preprint, 2023. DOI: 10.48550/arXiv.2304.13535.

20 M. F. Pusey, J. Barrett and T. Rudolph, *arXiv* preprint, 2011. DOI: 10.48550/ARXIV.1111.3328.

21 W. Liu, K. A. Pratte, P. J. Castaldi, C. Hersh, R. P. Bowler, F. Banaei-Kashani and K. J. Kechris, *PLOS Computational Biology*, **2025**, e1011842.

22 G. Nicora, F. Vitali, A. Dagliati, N. Geifman and R. Bellazzi, *Front. Oncol.*, 2020, **10**, 1030.

23 *Multimodal Optical Diagnostics of Cancer*, ed. V. V. Tuchin, J. Popp and V. Zakharov, Springer International Publishing, 2020.

24 V. M. Gun'ko, A. V. Klyueva, Y. N. Levchuk and R. Leboda, *Adv. Colloid Interface Sci.*, 2003, **105**, 201–328.

25 M. Steer, J. Picton and J. Earnshaw, *Advances in Botanical Research*, Elsevier, 1985, pp. 1–69.

26 W. Becker, A. Bergmann, G. L. Biscotti and A. Rueck, *Lasers and Applications in Science and Engineering*, 2004, p. 104.

27 M. Kress, *J. Biomed. Opt.*, 2003, **8**, 26.

28 K. A. Zachariasse, *Nachr. Chem., Tech. Lab.*, 1985, **33**, 896–896.

29 K. Yao, R. Unni and Y. Zheng, *Nanophotonics*, 2019, **8**, 339–366.

30 Z. A. Kudyshev, A. V. Kildishev, V. M. Shalaev and A. Boltasseva, *Nanophotonics*, 2020, **10**, 371–383.

31 J. Zhou, B. Huang, Z. Yan and J.-C. G. Bünzli, *Light: Sci. Appl.*, 2019, **8**, 84.

32 P. Virtanen, R. Gommers, T. E. Oliphant, M. Haberland, T. Reddy, D. Cournapeau, E. Burovski, P. Peterson, W. Weckesser, J. Bright, S. J. van der Walt, M. Brett, J. Wilson, K. J. Millman, N. Mayorov, A. R. J. Nelson, E. Jones, R. Kern, E. Larson, C. J. Carey, İ. Polat, Y. Feng, E. W. Moore, J. VanderPlas, D. Laxalde and D. Perktold, *Nat. Methods*, 2020, **17**, 261–272.

33 R. S. Hegde, *Nanoscale Adv.*, 2020, **2**, 1007–1023.

34 P. Freire, E. Manuylovich, J. E. Prilepsky and S. K. Turitsyn, *Adv. Opt. Photonics*, 2023, **15**, 739.

35 D. Liu, Y. Tan, E. Khoram and Z. Yu, *ACS Photonics*, 2018, **5**, 1365–1369.

36 S.-B. Wu, Z.-M. Li, J. Gao, H. Zhou, C.-S. Wang and X.-M. Jin, *Opt. Express*, 2023, **31**, 3479.

37 J. Gao, L.-F. Qiao, Z.-Q. Jiao, Y.-C. Ma, C.-Q. Hu, R.-J. Ren, A.-L. Yang, H. Tang, M.-H. Yung and X.-M. Jin, *Phys. Rev. Lett.*, 2018, **120**, 240501.

38 Z.-M. Li, S.-B. Wu, J. Gao, H. Zhou, Z.-Q. Yan, R.-J. Ren, S.-Y. Yin and X.-M. Jin, *Optica*, 2021, **8**, 323.

39 P. S. Emani, J. Warrell, A. Anticevic, S. Bekiranov, M. Gandal, M. J. McConnell, G. Sapiro, A. Aspuru-Guzik, J. T. Baker, M. Bastiani, J. D. Murray, S. N. Sotiropoulos, J. Taylor, G. Senthil, T. Lehner, M. B. Gerstein and A. W. Harrow, *Nat. Methods*, 2021, **18**, 701–709.

40 Z. A. Kudyshev, S. I. Bogdanov, T. Isacsson, A. V. Kildishev, A. Boltasseva and V. M. Shalaev, *Adv. Quantum Technol.*, 2020, **3**, 2000067.

41 V. Dunjko and H. J. Briegel, *arXiv* preprint, 2017. DOI: 10.48550/ARXIV.1709.02779.

42 A. A. Melnikov, H. Poulsen Nautrup, M. Krenn, V. Dunjko, M. Tiersch, A. Zeilinger and H. J. Briegel, *Proc. Natl. Acad. Sci. U. S. A.*, 2018, **115**, 1221–1226.

43 I. Cong, S. Choi and M. D. Lukin, *Nat. Phys.*, 2019, **15**, 1273–1278.

44 D. Bzdok, N. Altman and M. Krzywinski, *Nat. Methods*, 2018, **15**, 233–234.

45 Y. LeCun, Y. Bengio and G. Hinton, *Nature*, 2015, **521**, 436–444.

46 J. O. Berry, P. Yerramsetty, A. M. Zielinski and C. M. Mure, *Photosynth. Res.*, 2013, **117**, 91–120.

47 A. K. Biswal, G. K. Pattanayak, S. S. Pandey, S. Leelavathi, V. S. Reddy, G. Govindjee and B. C. Tripathy, *Plant Physiol.*, 2012, **159**, 433–449.

48 L. Y. Yang, L. T. Wang, J. H. Ma, E. D. Ma, J. Y. Li and M. Gong, *Photosynthetica*, 2017, **55**, 467–477.

49 R. Andersen and M. J. Kasperbauer, *Plant Physiol.*, 1973, **51**, 723–726.

50 S. Kuhlgert, G. Austic, R. Zegarac, I. Osei-Bonsu, D. Hoh, M. I. Chilvers, M. G. Roth, K. Bi, D. TerAvest, P. Weebadde and D. M. Kramer, *R. Soc. Open Sci.*, 2016, **3**, 160592.

51 S. O. Zakharkin, K. Kim, A. A. Bartolucci, G. P. Page and D. B. Allison, *Genomics, Proteomics Bioinf.*, 2006, **4**, 196–202.

52 J. M. Staub and P. Maliga, *Plant Cell*, 1992, **4**, 39–45.

53 M. H. Farkas, E. E. Mojica, M. Patel, D. S. Aga and J. O. Berry, *Analyst*, 2009, **134**, 1594.

54 P.-Y. Chen, *Mol. Breed.*, 2003, **11**, 287–293.

55 T. Thomay, S. V. Polyakov, O. Gazzano, E. Goldschmidt, Z. D. Eldredge, T. Huber, V. Loo and G. S. Solomon, *Phys. Rev. X*, 2017, **7**, 041036.

56 G. Xu, J. Carvalho, C. Wijesundara and T. Thomay, *APL Quantum*, 2024, **1**, 036122.

57 K. Inoue, E. Waks and Y. Yamamoto, *Phys. Rev. Lett.*, 2002, **89**, 037902.

58 C. Li, M. Ma, T. Zhang, P. Feng, X. Chen, Y. Liu, M. Brestic, T. M. Galal, H. M. Al-Yasi and X. Yang, *PLoS One*, 2021, **16**, e0255896.

59 G. Vico, F. Tang, N. Brunsell, T. Crews and G. Katul, *Agric. For. Meteorol.*, 2023, **341**, 109666.

60 N. Le, M. Zhang and K. Kim, *Int. J. Mol. Sci.*, 2022, **23**, 10763.

61 M. M. Barroso, *J. Histochem. Cytochem.*, 2011, **59**, 237–251.

62 F. Sotier, T. Thomay, T. Hanke, J. Korger, S. Mahapatra, A. Frey, K. Brunner, R. Bratschitsch and A. Leitenstorfer, *Nat. Phys.*, 2009, **5**, 352–356.

63 T. Thomay, T. Hanke, M. Tomas, F. Sotier, K. Beha, V. Knittel, M. Kahl, K. M. Whitaker, D. R. Gamelin, A. Leitenstorfer and R. Bratschitsch, *Opt. Express*, 2008, **16**, 9791.

64 M. Kahl, T. Thomay, V. Kohnle, K. Beha, J. Merlein, M. Hagner, A. Halm, J. Ziegler, T. Nann, Y. Fedutik, U. Woggon, M. Artemyev, F. Pérez-Willard, A. Leitenstorfer and R. Bratschitsch, *Nano Lett.*, 2007, **7**, 2897–2900.

65 M. Herrero-Collantes and J. C. Garcia-Escartin, *Rev. Mod. Phys.*, 2017, **89**, 015004.

66 M. Davanço, C. S. Hellberg, S. Ates, A. Badolato and K. Srinivasan, *Phys. Rev. B: Condens. Matter Mater. Phys.*, 2014, **89**, 161303.

67 Z. S. Tang, L. G. Helt and J. E. Sipe, *APL Quantum*, 2024, **1**, 036122.

68 I. I. Ozyigit and K. Yucebilgili Kurtoglu, *Mol. Biol. Rep.*, 2020, **47**, 9831–9847.

69 Bio-Rad Laboratories, *Helios Gene Gun System Instruction Manual*, Bio-Rad Laboratories, Hercules, California, USA, 2010.

70 E. Helenius, M. Boije, V. Niklander-Teeri, E. T. Palva and T. H. Teeri, *Plant Mol. Biol. Rep.*, 2000, **18**, 287–288.

71 J. Xia, A. Martinez, H. Daniell and S. N. Ebert, *BMC Biotechnol.*, 2011, **11**, 62.

72 B. Kuriakose, E. Du Toit and A. Jordaan, *S. Afr. J. Bot.*, 2012, **78**, 307–311.